2019 IEEE 58th Conference on Decision and Control (CDC)
Palais des Congrès et des Expositions Nice Acropolis
Nice, France, December 11-13, 2019

Isostable Reduction and Boundary Feedback Control for Nonlinear Convective Flows

Dan Wilson and Seddik Djouadi

Abstract— **A model reduction strategy using isostable coordinates is developed and applied to a prototype nonlinear convective flow past an obstacle. The flow is governed by the two-dimensional Burgers' equation subject to Dirichlet boundary controls. The Burgers' equation is used as a surrogate to the Navier-Stokes equations. The isostable coordinates are fully nonlinear and based on the infinite time convergence of transient behavior to a stationary solution. Linearization yields a model reduction strategy that explicitly accounts for the temporal dynamics of the underlying nonlinear flow and a strategy is developed for fitting observed data to the isostable reduced model. Open loop simulations of the isostable reduction outperform a previously validated nonlinear reduction strategy based on proper orthogonal decomposition. Additionally, the resulting isostable reduced framework is amenable for feedback control as demonstrated by solving a linear quadratic regulator problem in an isostable reduced coordinate system and applying the result to the full order system. To our knowledge, the use of isostable coordinates for reduced order modeling of fluid flows is novel.**

I. INTRODUCTION

Various applications such as drag reduction of road vehicles, airplanes, ships and submarines, drag reduction in pipes and air-conditioning systems, lift increase of airfoils, efficiency increase of harvesting wind and water energy, of heat transfer and of chemical and combustion processes [1][4][6], require the integration of feedback control because of the need for robustness to elements such as flight condition, vehicle attitude, precision tracking, and low fidelity models.

Unfortunately, models that capture the relevant dynamics of the input-output system and are amenable to control design are difficult to develop due to the to the extremely high order of these systems [2][3][4][5]. In particular, in certain applications such as in highly resolved flow solutions which require thousands of states, systematic development of feedback controls is a computationally intractable problem. The order of the system must be reduced before control design [20][9][11][2][3]. Much of this effort focuses on the proper orthogonal decomposition (POD) [7], Karhunen-Loeve expansion, or principal component analysis [5][6][1], clustering POD [13], spectral POD (SPOD) [14], balanced POD [5], and adaptive POD [15]. In [16][17] reduced order models based on POD have been obtained for linearized compressible flow equations. However, it is not clear how to extend these methods to nonlinear flows with high Reynolds numbers where the nonlinear terms dominate.

D. Wilson and S. Djouadi are with the Department of Electrical Engineering and Computer Science, University of Tennessee, Knoxville, TN 37996, USA dwilso81@utk.edu, mdjouadi@utk.edu

Dynamic mode decomposition (DMD) is a more recently developed data-driven flow decomposition designed to match stability eigenmodes under suitable conditions [1][6]. DMD trades the optimal resolution efficiency of POD against distillation of pure eigenfrequencies in short-time sampled data. DMD has a strong connection to the Koopman operator, which is an infinite dimensional linear operator describing the evolution of an observable function of a nonlinear dynamical system on a manifold [18][19][1]. Using Koopman based formalism, various data-driven techniques have been developed in order to identify representative reduced order linear models for that can be used to model the dynamics of nonlinear differential equations and subsequently apply active control [28][27][29].

In this paper, an alternative model reduction strategy using isostable coordinates is developed and applied to a prototype nonlinear convective flow past an obstacle. These isostable coordinates are related to level sets of the Koopman operator [22] and have been shown to be useful in other control applications [25][26]. The nonlinear convective flow problem, first proposed in [9], is governed by the two-dimensional Burgers' equation subject to Dirichlet boundary controls. The Burgers' equation, which has a convective nonlinearity like that in the Navier-Stokes momentum equations, is often used for the development of control methods relevant to flow control [9][10]. The isostable coordinates are fully nonlinear and based on the infinite time convergence of transient behavior to a stationary solution. Linearization yields a model reduction strategy that explicitly accounts for the temporal dynamics of the underlying nonlinear flow and a strategy is developed for fitting observed data to the isostable reduced model. Open loop simulations of the isostable reduction outperform a previously validated nonlinear reduction strategy based on proper orthogonal decomposition. Additionally, the resulting isostable reduced framework is amenable for feedback control as demonstrated by solving a simple linear quadratic regulator problem, as proposed in [20][8] in an isostable reduced coordinate system and applying the result to the full order system. While the notions of isostable coordinates and isostable reduction have been applied in other contexts [22][24][26], to our knowledge this technique has not been previously used for reduced order modeling of fluid flows.

II. PROTOTYPE PROBLEM: A NONLINEAR CONVECTIVE FLOW

Here we consider a prototype problem for a nonlinear convective flow past an obstacle as a testbed for the isostable

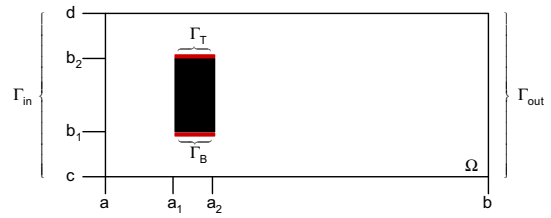

Fig. 1. Problem geometry is specified in the above figure. An identical geometry was considered in [20].

reduction methodology. As shown in Figure 1, we consider a rectangular domain $\Omega_1 \in \mathbb{R}^2$ given by $(a,b)\times(c,d)$ with a rectangular obstacle $\Omega_2 = [a_1,a_2]\times[b_1,b_2]$ so that the full domain is $\Omega = \Omega_1 \backslash \Omega_2$. Dirichlet boundary conditions are given on the top and bottom (Γ_T and Γ_B, respectively). An identical model was considered in [20]. The spatiotemporal dynamics are given by the two-dimensional Burgers' equation [20][11]

$$\frac{\partial}{\partial t}w(t,x,y) = \frac{1}{\mathrm{Re}}\Delta w(t,x,y) - \nabla\cdot F(w),$$
$$F(w) = \left[C_1\frac{w^2(t,x,y)}{2} \quad C_2\frac{w^2(t,x,y)}{2}\right]^T. \tag{1}$$

Here $C_1 = 1$ and $C_2 = 0$ are constants which determine the magnitude of the horizontal and vertical convection, respectively, Re is the counterpart of the Reynolds number from the Navier-Stokes equation, and $w(t,x,y)$ is the solution to the nonlinear PDE. For simplicity, boundary conditions on the top and bottom of the obstacle are assumed to be separable in space and time

$$w(t,\Gamma_T) = u_T(t)\Upsilon_T(x), \quad w(t,\Gamma_B) = u_B(t)\Upsilon_B(x). \tag{2}$$

The inflow, outflow, and remaining boundary conditions, Γ_{in}, Γ_{out} and Γ_u, respectively are

$$w(t,\Gamma_{in}) = f(y), \ \frac{\partial}{dx}w(t,\Gamma_{out}) = 0, \ w(t,\Gamma_u) = 0, \tag{3}$$

where $f(y)$ is a parabolic inflow.

III. Model Reduction Using Isostable Coordinates

Intuitively, isostable coordinates give a sense of the time it takes for an initial condition to approach its associated attractor. A formal definition was presented in [22] for use with ordinary differential equations (ODEs) where its relation to the Koopman operator was highlighted. Subsequent investigation of isostable coordinates for reduced order control strategies is presented in [25] for ODEs and in [26] for partial differential equations (PDEs). The notion of using isostable coordinates for reduced order control is perhaps most closely related to techniques involving inertial manifolds [21] (or transient attractors [23]), i.e., exponentially attracting, finite dimensional manifolds to which solutions rapidly collapse. However, a significant benefit of using isostable methods is that they do not require a large spectral gap between consecutive eigenvalues.

To begin, consider a PDE on some domain Ω

$$\frac{\partial}{\partial t}X(r,t) = F(X(r,t),r) + G(X(r,t)), \tag{4}$$

with boundary control

$$X(\partial\Omega,t) = f_0(\partial\Omega) + f_1(\partial\Omega,t). \tag{5}$$

Equation (5) specifies Dirichlet boundary conditions, but both Neumann or mixed boundary conditions could also be specified. In the above equations, $X(r,t) \in \mathbb{R}^m$ is the state at location r and time t, F gives the local dynamics, G represents spatial coupling, (e.g. advection or diffusion), $f_0(\partial\Omega)$ gives the nominal boundary conditions on the boundary $\partial\Omega$ and $f_1(\partial\Omega,t)$ is a time dependent control. It will be assumed that when $f_1(\partial\Omega,t) = 0$ (i.e., in the absence of boundary control) that a stationary solution $X_{SS}(r)$ of (4) exists that satisfies $F(X_{SS}(r),r) + G(X_{SS}(r)) = 0$. Additionally, for the nominal boundary conditions, we will assume that $J \equiv \nabla[F(X_{SS}(r),r) + G(X_{SS}(r))]$ exists and is a compact operator. Here, J is a local linearization of (4) evaluated at the stationary solution.

Isostable coordinates will be defined as in [26]. These coordinates represent the asymptotic convergence of initial conditions in the basin of attraction of the stationary solution X_{SS}. Note here that these coordinates are defined with respect to the nominal boundary conditions (i.e., taking $f_1(\partial\Omega,t)$ = 0). Additionally, we will suppose that solutions of (4) near the stationary solution can be written to leading order accuracy as an infinite sum of eigenfunctions, $\phi_j(r)$ of J with associated eigenvalues λ_j

$$X(r,t) - X_{SS} = \sum_{j=1}^{\infty} s_j[X(r,0) - X_{SS}]\phi_j(r)e^{\lambda_j t}. \tag{6}$$

Here $s_j(X)$ represent the coordinates of X in the basis of the eigenfunctions, $X(r,0)$ is the initial state, and the eigenvalues are sorted according to $0 \geq \mathrm{Re}(\lambda_j) \geq \mathrm{Re}(\lambda_{j+1})$ so that λ_1 corresponds to the eigenfunction with the slowest rate of decay. This eigenfunction basis is used to define isostable coordinates in the basin of attraction of the stationary solution [26]

$$\Psi_j\{X(r)\} = \lim_{t\to\infty} e^{-\lambda_j t}\int_\Omega Q_j^T(r)(X(r,t) - X_{SS})dr, \tag{7}$$

where Q_j projects the solution onto $\phi_j(r)$, i.e., $\int_\Omega Q_j^T(r)\phi_k(r)dr = 1$ for $k = j$ and 0 for $k \neq j$. Note that the eigenfunctions $\phi_j(r)$ are not generally orthogonal to each other; consequently Q_j and ϕ_j are usually different. The relationship between isostable coordinates and level sets of the Koopman operator was noted established in [22] in ODEs.

A. Dynamics of Isostable Coordinates

The definition of isostable coordinate is particularly useful because $\int_\Omega Q_j^T(r)(X(r,t) - X_{SS})dr \propto \phi_j(r)e^{\lambda_j t}$ as $t \to \infty$. This relationship can be used to show that (as in [26])

$$\frac{d\Psi_j\{X(r,t)\}}{dt} = \lambda_j\Psi_j\{X(r,t)\}. \tag{8}$$

Equation (8) states that without boundary control, isostable coordinates decay exponentially towards zero. Recall that for states close to the stationary solution, to leading order accuracy

$$\begin{aligned} X(r,0)-X_{SS} &= \sum_{j=1}^{\infty} s_j[X(r,0)-X_{SS}]\phi_j(r) \\ &= \sum_{j=1}^{\infty} \Psi_j\{X(r,0)\}\phi_j(r). \end{aligned} \tag{9}$$

In the second line in the above equation, the relationship $s_j[X(r,0)-X_{SS}] = \Psi_j\{X(r,0)\}$ is used which can be shown using the definition of isostable coordinates from (7). For convenience of notation in the following analysis, we will drop the dependence of Ψ_j on X and write it solely as a function of time. Equation (9) is valid for any initial conditions which implies

$$Y(r,t) = \sum_{j=1}^{\infty} \Psi_j(t)\phi_j(r), \tag{10}$$

where $Y(r,t) \equiv X(r,t)-X_{SS}$ is the observed output.

For the model (1), the effect of boundary control for small inputs (i.e., when $w(t,\Gamma_T)$ and $w(t,\Gamma_B)$ are order ε terms with $0<\varepsilon\ll 1$) can be understood with the following derivation. First, taking the inner product of both sides of (1) with $Q_j(x,y)$ as defined in (7) yields

$$\begin{aligned} \int_\Omega \frac{\partial}{\partial t} w(t,x,y)Q_j(x,y)dxdy = \\ -\frac{1}{2}\int_\Omega \left[\frac{\partial}{\partial x}w^2(t,x,y)\right] Q_j(x,y)dxdy \\ +\frac{1}{\mathrm{Re}}\int_\Omega [\Delta w(t,x,y)]\, Q_j(x,y)dxdy. \end{aligned} \tag{11}$$

Manipulating (11) using Green's identities yields

$$\begin{aligned} \int_\Omega \frac{\partial}{\partial t} w(t,x,y)Q_j(x,y)dxdy = \\ -\frac{1}{2}\int_\Omega \left[\frac{\partial}{\partial x}w^2(t,x,y)\right] Q_j(x,y)dxdy \\ -\frac{1}{\mathrm{Re}}\int_\Omega \nabla w(t,x,y)\cdot\nabla Q_j(x,y)dxdy \\ +\frac{1}{\mathrm{Re}}\int_{\partial\Omega} Q_j(x,y)\nabla w(t,x,y)\cdot ndS(x,y). \end{aligned} \tag{12}$$

where n is a unit vector oriented normal to the surface element dS. To proceed, we let $f_\beta^j(x,y,t) \equiv -\frac{1}{2}\int_\Omega \left[\frac{\partial}{\partial x}w^2(t,x,y)\right] Q_j(x,y)dxdy - \frac{1}{\mathrm{Re}}\int_\Omega \nabla w(t,x,y)\cdot\nabla Q_j(x,y)dxdy$. Here $f_\beta^j(x,y,t)$ consists of all terms of (13) that do not depend on the flux across the boundary, and hence do not respond directly to the boundary control. For the remaining terms of (13), we use the results from (9)

$$\begin{aligned} \int_\Omega \frac{\partial}{\partial t}\left[w_{SS}(x,y)+\sum_{k=1}^{\infty}\Psi_k(t)\phi_k(x,y)\right] Q_j(x,y)dxdy = f_\beta^j(x,y,t) \\ +\frac{1}{\mathrm{Re}}\int_{\partial\Omega} Q_j(x,y)\nabla w(t,x,y)\cdot ndS(x,y), \end{aligned} \tag{13}$$

where $w_{SS}(x,y)$ denotes the steady state solution. We simplify the left hand side of the above equation by recalling that $\int_\Omega Q_j(x,y)\phi_k(x,y)dxdy = 1$ for $k=j$ and 0 otherwise. This yields

$$\Psi_j = f_\beta^j(x,y,t) + \frac{1}{\mathrm{Re}}\int_{\partial\Omega} Q_j(x,y)\nabla w(t,x,y)\cdot ndS(x,y). \tag{14}$$

The boundary integral from (14) can be simplified using the boundary equations from (3); the solution of (1) along Γ_u and Γ_{out} is specified to be zero resulting in

$$\begin{aligned} \int_{\partial\Omega} Q_j(x,y)\nabla w(t,x,y)\cdot ndS(x,y) = \\ \int_{a_1}^{a_2}\left(\frac{\partial}{\partial y}w(t,x,b_1)Q_j(x,b_1) - \frac{\partial}{\partial y}w(t,x,b_2)Q_j(x,b_2)\right)dx \\ +\int_a^b\left(\frac{\partial}{\partial y}w(t,x,d)Q_j(x,d) - \frac{\partial}{\partial y}w(t,x,c)Q_j(x,c)\right)dx \\ +\int_{b_1}^{b_2}\left(\frac{\partial}{\partial y}w(t,a_1,y)Q_j(a_1,y) - \frac{\partial}{\partial y}w(t,a_2,y)Q_j(a_2,y)\right)dy \\ -\int_c^d \frac{\partial}{\partial x}w(t,a,y)Q_j(a,y)dy. \end{aligned} \tag{15}$$

Partial derivatives in (15) that are influenced by the boundary control can be approximated for $h>0$ as

$$\begin{aligned} \frac{\partial}{\partial y}w(t,x,b_1) &\approx \frac{u_B(t)\Upsilon_B(x) - w(t,x,b_1-h)}{h}, \\ \frac{\partial}{\partial y}w(t,x,b_2) &\approx \frac{w(t,x,b_2+h) - u_T(t)\Upsilon_T(x)}{h}. \end{aligned} \tag{16}$$

Taking the results of (16) and (15), substituting them into (14) yields

$$\Psi_j = f_j^{nbc}(t,x,y) + \alpha_{j,1}u_T(t) + \alpha_{j,2}u_B(t), \tag{17}$$

where $\alpha_{j,1} = \frac{1}{h\mathrm{Re}}\int_{a_1}^{a_2} Q_j(x,b_2)\Upsilon_T(x)dx$, $\alpha_{j,2} = \frac{1}{h\mathrm{Re}}\int_{a_1}^{a_2} Q_j(x,b_1)\Upsilon_B(x)dx$, and $f_j^{nbc}(t,x,y)$ is the summation of all terms that do not depend on either of the boundary controls. Recalling from (8) that $\dot\Psi_j = \lambda_j\Psi_j$ in the absence of boundary control, this implies that for small enough h, $f_j^{nbc}(t,x,y)$ is well approximated by $\lambda_j\Psi_j$. Furthermore, the analysis can be repeated for all isostable coordinates and we write

$$\dot\Psi_j = \lambda_j\Psi_j + \alpha_{j,1}u_T(t) + \alpha_{j,2}u_B(t), \quad j=1,2,\ldots. \tag{18}$$

B. Fitting a Reduced Model to Data

Here, we provide a strategy to estimate the constants $\alpha_{j,k}$ from (18) from observed behavior. To begin, suppose we have M independent boundary inputs yielding a more general version of (18)

$$\dot\Psi_j = \lambda_j\Psi_j + \sum_{k=1}^{M}\alpha_{j,k}u_k(t), \quad j=1,2,\ldots. \tag{19}$$

A subset of the isostable coordinates will be fit to a reduced NM-dimensional model of the form

$$\begin{aligned} \dot\Psi_{j,k} = \lambda_j\Psi_{j,k} + \alpha_{j,k}u_k(t) \\ j=1,\ldots,N, \quad k=1,\ldots,M, \end{aligned} \tag{20}$$

i.e., using N isostable coordinates associated with eigenvalues $\lambda_1,\ldots,\lambda_N$ which have the smallest real component. The rational behind this choice is that perturbations to the truncated isostable coordinates will decay quickly and will not have a lasting effect on the dynamical behavior. The strategy of neglecting isostable coordinates which decay rapidly has been used successfully in other applications [25][26], however, the models used in these examples were simple enough so that the reduced equations could be calculated numerically using an "adjoint equation". In the above equation, each input receives its own set of isostable coordinates to allow for the possibility of repeated eigenvalues in (8). The state to output relationship for (20) follows

$$Y(x,y,t)=\sum_{k=1}^{M}\sum_{j=1}^{N}\phi_{j,k}(x,y)\Psi_{j,k}(t). \tag{21}$$

The ultimate goal here is to infer the coefficients $\alpha_{j,k}$ and eigenfunctions $\phi_{j,k}(x,y)$ given knowledge of the eigenvalues λ_j. To do so, consider the following control input: $u_k(t)=\rho\sin(\omega t)$ where ρ is a small constant. With this input, the steady state behavior of (20) (and corresponding output) can be found analytically:

$$\begin{aligned}\Psi_j^{ss}(t)&=\frac{-\rho\alpha_{j,k}}{\omega^2+\lambda_j^2}\left(\lambda_j\sin(\omega t)+\omega\cos(\omega t)\right),\\ Y^{ss}(x,y,t,\omega)&=\sum_{j=1}^{N}\frac{-\rho\alpha_{j,k}\phi_{j,k}(x,y)}{\omega^2+\lambda_j^2}\left(\lambda_j\sin(\omega t)+\omega\cos(\omega t)\right).\end{aligned} \tag{22}$$

The above relationship is valid for any choice of ω, and therefore yields the following strategy for finding the unknown eigenfunctions: **1)** Apply a sinusoidal input $u_k(t)=\rho\sin(\omega_i t)$ **2)** Measure the steady state output $Y^{ss}(x,y,t,\omega)$ at all locations of interest. **3)** Repeat steps 1 and 2 for inputs with q different frequencies where $q>N$. **4)** Obtain an estimate for the eigenfunctions according to the relationship

$$\begin{bmatrix}\alpha_{1,k}\phi_{1,k}(x,y)\\ \vdots\\ \alpha_{N,k}\phi_{N,k}(x,y)\end{bmatrix}=-\frac{2}{\rho}\Sigma^{\dagger}\begin{bmatrix}\frac{1}{T}\int_0^T Y^{ss}(x,y,t,\omega_1)\sin(\omega_1 t)dt\\ \vdots\\ \frac{1}{T}\int_0^T Y^{ss}(x,y,t,\omega_q)\sin(\omega_q t)dt\end{bmatrix}, \tag{23}$$

where the element in the i^{th} row and j^{th} column of $\Sigma\in\mathbb{R}^{q\times N}$ is equal to $\lambda_j(\omega_i^2+\lambda_j^2)^{-1}$, and † denotes the pseudoinverse. Intuitively, (23) provides a least squares fit for the unknown coefficients. **5)** Repeat steps 1-4 to calculate $\alpha_{j,k}\phi_{j,k}$ for all j and k. **6)** Because $\alpha_{j,k}$ and $\phi_{j,k}$ cannot be resolved individually, define scaled variables and eigenfunctions $\overline{\Psi}_{j,k}=\Psi_{j,k}/\alpha_{j,k}$ and $\overline{\phi}_{j,k}=\phi_{j,k}\alpha_{j,k}$. Starting with (20) and (21), a coordinate transformation yields the state space representation

$$\begin{aligned}\frac{d\overline{\Psi}_{j,k}}{dt}&=-\lambda_j\overline{\Psi}_{j,k}+u_k(t),\\ &\quad j=1,\ldots,N,\quad k=1,\ldots,M,\\ Y(x,y,t)&=\sum_{j=1}^{N}\sum_{k=1}^{M}\overline{\phi}_{j,k}(x,y)\overline{\Psi}_{j,k}(t).\end{aligned} \tag{24}$$

IV. Reduction and Control Applied to Nonlinear Convective Flow

In the following simulations, $\Omega_1=(0,0.99]\times(0,0.48]$, $\Omega_2=[0.15,0.24]\times[0.15,0.33]$ with a uniform spatial step of $h=0.015$ yielding 1955 states in the discretized model. Letting $\text{Re}=300$ and taking the inflow $f(y)=-625y^2/36+25y/3$ (so that the $\max_y(f(y))=1$) yields the steady state distribution shown in Figure 2A. The eigenvalues corresponding to the temporal decay of transient behavior towards the stationary solution are estimated by spatially discretizing (1), taking the Jacobian of the resulting equations evaluated at the stationary solution, and calculating the eigenvalues of the resulting matrix. Eigenvalues with the 30 smallest magnitude real components (and hence slowest decay) are shown in Figure 2D. The first 9 eigenvalues are real numbers. Using the methodology presented in Section III-B, The model (1) is simulated taking $\Upsilon_T(x)=\Upsilon_B(x)=1$ with inputs $u_T(t)=0.3\sin(\omega t)$ for 61 values of ω ranging from 0.3 to 6.3. The resulting steady state behavior is used to fit a model with the first 6 eigenvalues (red dots from the bottom panel of Figure 2). The same procedure is repeated taking $u_B(t)=0.3\sin(\omega t)$. The resulting isostable modes $\phi_{1,a}$ through $\phi_{3,a}$ (resp., $\phi_{1,b}$ through $\phi_{3,b}$) corresponding to boundary control on the top (resp., bottom) surface of the obstacle are shown in Figure 2B, (resp. 2C). These modes (and higher modes that are not shown) all have approximately the same shape, but different magnitudes and decay rates.

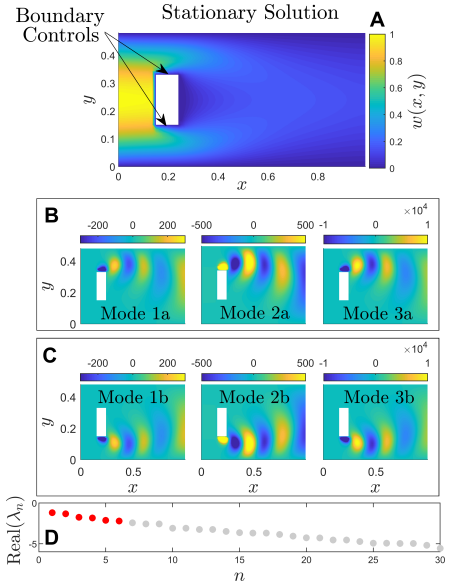

Fig. 2. Panel A shows the stationary solution for $\text{Re}=300$. Panels B and C show a subset of the isostable reduced modes associated with boundary control on the top and bottom surface of the obstacle, respectively. The 30 eigenvalues with the smallest magnitude real components (and hence slowest decay) are shown in panel D. Six eigenvalues per control input are used to obtain resulting modes in panels B and C.

The efficacy of the isostable reduction framework is compared to a reduction strategy using proper orthogonal decomposition (POD) [20], a well established, model independent technique used to represent simulation (or experimental) data

using an optimal set of modes in an L^2 energy sense. We implement the same method used in [20], whereby a set of snapshots is generated by numerical simulation of (1) for different time-varying boundary inputs and the resulting data is used to construct the POD basis. There are 20 resulting modes required to capture 99.9 percent of the resulting energy

A. Comparison Between Open-Loop Simulations

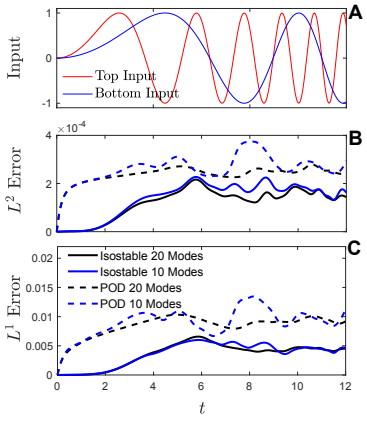

Fig. 3. Panel A shows an open-loop boundary control applied to the model. Panel B (resp., C) shows how the resulting L^2 (resp., L^1) error between the full model solution and the reduced model solution changes over time. By both measures of error, the isostable based model results in significantly better agreement, even while using fewer modes.

Direct comparisons of the full model to the reduced isostable and POD based reduced models are shown in Figure 3. The isostable coordinate dynamics are simulated according to (20) with the state mapped to the output behavior according to (21). The dynamics of the POD reduced model are taken to be identical to the nonlinear reduced model derived in [20]. Figure 3A shows an example open-loop boundary input applied to the top and bottom of the obstacle and the resulting L^2 and L^1 error (panel 3B and 3C, respectively) between full and respective reduced model solutions. For this and other open-loop inputs (not shown) the isostable reduced model significantly outperforms the POD based model, even when fewer modes are used.

B. Feedback Control Using Isostable Methods

The system from (24) can be represented with the state space equations

$$\dot{d} = Ad + Bu, \tag{25}$$

where d is a vector comprised of each $\Psi_{j,k}$, u accounts for each separate control input, and A and B are appropriately sized matrices. For this system we will consider a tracking problem whereby a target reference solution $w(x,y)_{\text{ref}}$ is specified for the PDE (1). This solution is projected onto an 8 mode isostable basis for the Re $= 300$ simulations yielding tracking coefficients d_{ref}. The augmented state-space equations can be written as

$$\begin{aligned}\begin{bmatrix}\dot{d}\\ \dot{d}_{\text{ref}}\end{bmatrix} &= \begin{bmatrix}A & 0\\ 0 & 0\end{bmatrix}\begin{bmatrix}d\\ d_{\text{ref}}\end{bmatrix} + \begin{bmatrix}B\\ 0\end{bmatrix}u\\ &= \bar{A}D + \bar{B}u.\end{aligned} \tag{26}$$

Following a similar setup to [20][8] in order to provide a direct comparison, a control problem can be formulated using the γ-shifted linear quadratic regulator (LQR) cost function

$$J_c(d(0),u,d_{\text{ref}}) = \int_0^\infty \left[(d-d_{\text{ref}})^T Q(d-d_{\text{ref}}) + u^T R u\right] e^{2\gamma t}\,dt, \tag{27}$$

where Q and R are both diagonal and positive semi-definite and represent the state and control weights, respectively, and $\gamma \in \mathbb{R}^+$ provides robustness to the resulting controller. The optimal control problem to be considered is to minimize J_c over all possible controls $u \in L^2(0,\infty)$ subject to the state-space dynamics (26).

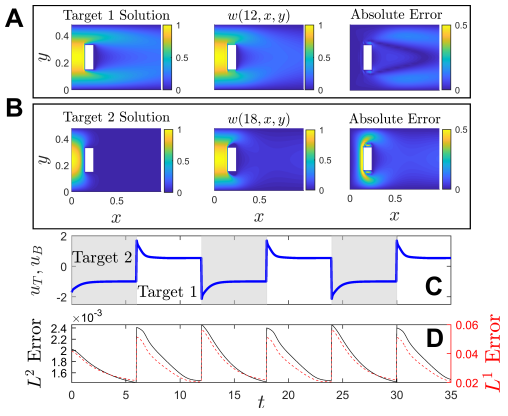

Fig. 4. From left to right, panel A (resp. B) shows the first (resp. second) target solution, the controlled solution at $t = 12$ (resp. t = 18), right before the target solutions switch, and the absolute error between the target and actual solutions is shown in the far right panel. Panel C shows the control magnitude on both the top and bottom of the obstacle. Targets 1 and 2 when the background of panel C is white and gray, respectively. The error between the target solutions and the actual solution is shown in panel D.

As detailed in [20], the LQR optimization problem has a unique solution

$$u_{\text{opt}} = -KD, \tag{28}$$

so that the resulting closed loop system follows

$$\dot{D} = (\bar{A} - \bar{B}K)D, \tag{29}$$

where,

$$K = \begin{bmatrix}R^{-1}B^T\Pi_1 & R^{-1}B^T\Pi_2\end{bmatrix}. \tag{30}$$

In the feedback law, Π_1 is the solution to the algebraic Riccati equation

$$(A+\gamma I)^T\Pi_1 + \Pi_1(A+\gamma I) - \Pi_1 B R^{-1} B^T \Pi_1 + Q = 0, \tag{31}$$

and Π_2 solves

$$\left[(A+\gamma I)^T - \Pi_1 B R^{-1} B^T\right]\Pi_2 = Q. \tag{32}$$

This feedback control strategy is implemented using two target solutions, the first being the steady state solution when $\mathrm{Re} = 600$, and the second being the steady state solution when $\mathrm{Re} = 50$. These targets are shown in Figures 4A and 4B, respectively. In order to implement this control strategy for the full model, the K matrix from (30) is first calculated taking Q and R to be appropriately sized identity matrices. Next, target solutions 1 and 2 are projected onto a basis of modes of the isostable reduction to determine d_{ref} for each solution. The full model (1) is then simulated and the boundary control is determined using (28) where at each instant in time, d determined by projecting the current state onto the set of isostable modes. After every 6 units of time, the target solutions are interchanged, and results are shown in Figure 4. While this system is highly underactuated, the controller is successful at tracking the reference functions. Figure 4C shows the top and bottom control input which are identical. Panel D shows the L^2 and L^1 errors between the targets and the resulting full model solutions as black and dashed-red lines, respectively. Note here that the error is calculated at locations to the right of the obstacle (i.e., where $x > a_2$); this choice is made because in this example boundary control has a negligible influence on the solution left of the obstacle.

V. Conclusion

In this paper, an isostable based reduction strategy is developed for a nonlinear convective system similar to the Navier-Stokes equations. A strategy for inferring the reduced model behavior from model data is also suggested. This strategy is compared to another reduction strategy based on POD and was found to replicate model features better than the nonlinear POD based reduced model. Additionally, the isostable reduced model outperforms the POD reduction while using significantly fewer modes. Successful feedback control was implemented using the isostable reduced model control framework when applied to the full order, nonlinear system.

References

[1] S. L. Brunton and B. R. Noack, Closed-Loop Turbulence Control: Progress and Challenges. *Applied Mechanics Reviews*, pp. 1–48, vol. 67, Sept. 2015.

[2] C.W. Rowley and B.A. Batten, Dynamic and Closed-Loop Control. In *Fundamentals and Applications of Modern Flow Control*, R.D. Joslin and D.N. Miller, editors, vol. 231, Progress in Astronautics and Aeronatics, AIAA, 2009.

[3] C.W. Rowley and D.R. Williams, Dynamics and Control of High-Reynolds-Number Flow over Open Cavities, Annu. Rev. Fluid Mech., vol. 38, pp. 251-276, 2006.

[4] M. Samimy, M. Debiasi, E. Caraballo, A. Serrani, X. Yuan, J. Little and J. H. Myatt, Feedback control of subsonic cavity flows using reduced-order models, J. Fluid Mech. (2007), vol. 579, pp. 315-346.

[5] C.W. Rowley and S.T.M. Dawson, Model Reduction for Flow Analysis and Control. Annual Review of Fluid Mechanics, vol. 49, pp. 387-417, 2017.

[6] K. Taira, S.L. Brunton, S. Dawson, C.W. Rowley, T. Colonius, B.J. McKeon, O.T. Schmidt, S. Gordeyev, V. Theofilis, and L.S. Ukeiley. Modal analysis of fluid flows: An overview. AIAA J. vol. 55. no. 12, pp. 4013-4041, 2017.

[7] Holmes, P., Lumley, J., and Berkooz, G., *Turbulence, Coherent Structures, Dynamical Systems and Symmetry*, Cambridge University Press, New York, 1996, pp. 86-127.

[8] R.C. Camphouse. Boundary Feedback Control Using Proper Orthogonal Decomposition Models, *Journal of Guidance, Control, and Dynamics*, Vol. 28, No. 5, September-October 2005, pp 931-938.

[9] C.R. Camphouse and J. Myatt, Feedback Control for a Two-Dimensional Burgers' Equation System Model, AIAA Paper 2004-2411, June 2004.

[10] J. A. Burns and S. Kang, A Stabilization Problem for Burgers' Equation with Unbounded Control and Observation. Control and Estimation of Distributed Parameter Systems, edited by F. Kappel, K. Kunisch, and W. Schappacher, Vol. 100, Birkhauser Verlag, 1991, pp. 51-72.

[11] R.C. Camphouse, S.M. Djouadi and J.H. Myatt, Feedback Control for Aerodynamics, Proceedings of the 46th lEEE Conference on Decision and Control, San-Diego, pp. 4579-4590, 2006.

[12] S.M. Djouadi, R.C. Camphouse and J.H. Myatt, Optimal Order Reduction for the Two-Dimensional Burgers' Equation, IEEE Control and Decision Conference, NO, pp. 3507-3512, 2007.

[13] S. Sahyoun and S.M. Djouadi, Local Proper Orthogonal Decomposition Based on Space Vectors Clustering, International Conference on Systems and Control, Algiers, Algeria, September 2013, pp. 665 - 670.

[14] A. Towne, O.T. Schmidt, and T. Colonius, Spectral proper orthogonal decomposition and its relationship to dynamic mode decomposition and resolvent analysis. Journal of Fluid Mechanics, vol. 847, pp. 821-867, 2018.

[15] A. Varshney, S. Pitchaiah, and A. Armaou, Fedback Control of Dissipative PDE Systems using Adaptive Model Reduction, AIChE Journal, vol. 55, No. 4, April 2009, pp. 906-918.

[16] I. Kalashnikova, S. Arunajatesan, A Stable Galerkin Reduced Order Model (ROM) for Compressible Flow. WCCM Paper No. 2012-18407, 10th World Congress for Computational Mechanics (WCCM), Sao Paulo, Brazil, July 2012.

[17] M.F. Barone, I. Kalashnikova, D.J. Segalman, H. Thornquist, Stable Galerkin Reduced Order Models for Linearized Compressible Flow. J. Comput. Phys. 288, pp. 1932–1946, 2009.

[18] C.W. Rowley, I. Mezic, S. Bagheri, P. Schlatter, and D. Henningson. Spectral Analysis of Nonlinear Flows, J. Fluid Mech., vol. 645, pp. 115-127, 2009.

[19] J.H. Tu, C.W. Rowley, D.M. Luchtenburg, S.L. Brunton, and J.N. Kutz. On Dynamic Mode Decomposition: Theory and Applications, J. Comput. Dyn., vol. 1. no.2, pp. 391-421, 2014.

[20] R. C. Camphouse and J. Myatt. Reduced order modelling and boundary feedback control of nonlinear convection. In *AIAA Guidance, Navigation, and Control Conference*, page 5844, 2005.

[21] C. Foias, G. R. Sell, and R. Temam. Inertial manifolds for nonlinear evolutionary equations. *Journal of Differential Equations*, 73(2):309–353, 1988.

[22] A. Mauroy, I. Mezić, and J. Moehlis. Isostables, isochrons, and Koopman spectrum for the action–angle representation of stable fixed point dynamics. *Physica D: Nonlinear Phenomena*, 261:19–30, 2013.

[23] A. J. Roberts. Appropriate initial conditions for asymptotic descriptions of the long term evolution of dynamical systems. *The Journal of the Australian Mathematical Society. Series B. Applied Mathematics*, 31(01):48–75, 1989.

[24] D. Wilson and B. Ermentrout. Greater accuracy and broadened applicability of phase reduction using isostable coordinates. *Journal of Mathematical Biology*, 76(1-2):37–66, 2018.

[25] D. Wilson and J. Moehlis. Extending phase reduction to excitable media: Theory and applications. *SIAM Review*, 57(2):201–222, 2015.

[26] D. Wilson and J. Moehlis. Isostable reduction with applications to time-dependent partial differential equations. *Physical Review E*, 94(1):012211, 2016.

[27] H. Arbabi, M. Korda, and I. Mezić. A data-driven koopman model predictive control framework for nonlinear partial differential equations. In *2018 IEEE Conference on Decision and Control*, pages 6409–6414. IEEE, 2018.

[28] E. Kaiser, N. J. Kutz, and S. L. Brunton. Data-driven discovery of koopman eigenfunctions for control. *arXiv preprint arXiv:1707.01146*, 2017.

[29] S. Peitz and S. Klus. Koopman operator-based model reduction for switched-system control of PDEs. *Automatica*, 106:184–191, 2019.